

Original Article

Mechanical properties of aramid fiber-reinforced composites and performance on repairing concrete beams damaged by corrosion

Pitcha Jongvivalsakul¹, Chung Nguyen Thi², Ganchai Tanapornraweekit³,
and Linh Van Hong Bui^{4*}

¹ *Innovative Construction Materials Research Unit, Department of Civil Engineering, Faculty of Engineering, Chulalongkorn University, Pathum Wan, Bangkok, 10330 Thailand*

² *Department of Civil Engineering, Faculty of Engineering, Chulalongkorn University, Pathum Wan, Bangkok, 10330 Thailand*

³ *Construction and Maintenance Technology Research Center, School of Civil Engineering and Technology, Sirindhorn International Institute of Technology, Thammasat University, Khlong Luang, Pathum Thani, 12120 Thailand*

⁴ *Faculty of Civil Engineering, Industrial University of Ho Chi Minh City, Go Vap, Ho Chi Minh, Viet Nam*

Received: 30 January 2019; Accepted: 16 March 2019

Abstract

This study presents an experimental investigation of the mechanical responses of concrete members with partially aramid fiber-reinforced concrete (AFRC). The effect of fiber geometry on mechanical properties of AFRC was investigated to provide a reasonable dimension of the aramid fibers for reinforcing the concrete beams. Additionally, an experiment on the flexural behavior of corroded reinforced concrete (RC) beams repaired by aramid fiber-reinforced mortar or high performance mortar was carried out. The test results indicated that 40 mm is the best fiber length to maximize the tensile strength of AFRC. Furthermore, the twisted fibers can resist a higher load capacity in the post-peak regions than single fibers. Both non-repaired and repaired RC beams were tested under a four-point bending load. The experimental results demonstrated that the load capacity and the ductility of a repaired corroded RC beam using aramid fiber-reinforced mortar were restored almost to the same capacity as a non-corroded RC member. The width of cracks in the corroded beam repaired with aramid fibers decreased significantly.

Keywords: aramid fiber, fiber geometry, corrosion, repairing, flexural capacity

1. Introduction

Corrosion damage to reinforced concrete (RC) structures is a serious problem and has recently received world-wide attention. Most of previous research reported that corrosion of the steel reinforcement in RC members reduced the flexural strength and increased the deflection of RC members (Maaddawy *et al.*, 2005; Chung *et al.*, 2008). Therefore, to avoid corrosion of the steel reinforcement in a

RC structure, the addition of discontinuous fibers into the concrete was proposed by Altun *et al.* (2007), Mansour *et al.* (2011), and Yoo *et al.* (2015). This also resulted in the improvement of stiffness (Iqbal *et al.*, 2016) and flexural/shear capacity (Kim *et al.*, 2016; Jongvivalsakul *et al.*, 2011) of the members.

Aramid fiber is a type of synthetic fiber that has high tensile strength, modulus of elasticity, heat resistance, and chemical resistance. There are a number of practical applications for aramid fibers in actual structures. However, as reported in past work (Linh *et al.*, 2017; Linh *et al.*, 2018) the members with aramid fiber-reinforced concrete (AFRC) exhibited less ductility compared with members reinforced by

*Corresponding author

Email address: buivanhonglinh@iuh.edu.vn

steel. Therefore, repair of concrete beams by replacing with partially AFRC is considered to enhance the ductility, strength, and durability of the existing structures compared to members with single fiber-reinforced concrete.

Currently, it seems that only a study by Soroushian *et al.* (1990) investigated the effects of the volume fraction and length of fibers on the strength and toughness of AFRC composites. Their study showed that the service strength and ductility drastically improved when aramid fibers were used for reinforcement of cement composites. However, that work tested only fiber lengths that ranged from 3 to 12.7 mm. To date, longer macro-fiber lengths more than 30 mm have not been studied. Thus, it is difficult to propose the optimum fiber length and fiber configuration for the practical use of aramid macro-fiber. Furthermore, although the aramid fiber is a non-corrodible material, the application and the study of the aramid fibers as repair material for corroded RC beams have not been given much attention.

In this study, elementary tests were carried out to investigate the effects of fiber length and fiber shape on the mechanical properties of aramid fiber-reinforced concrete. Concrete specimens reinforced with aramid fiber lengths of 30 mm, 40 mm, and 50 mm among the single and twisted aramid fibers were tested. The effectiveness of aramid fibers as a repair material was examined for application in the second part of this study. The experimental results of four types of RC beams are presented: (1) non-damaged, (2) damaged, (3) damaged and repaired by aramid fiber-reinforced mortar (AFRM), and (4) damaged and repaired by high performance mortar. The flexural performances were analyzed by means of the load-deflection relationship and cracking mechanism of all beams. This research provides insight into the behaviors of the members repaired by AFRC in a harsh environment and provides a reliable database for future studies.

2. Mechanical properties of aramid fiber-reinforced concrete (AFRC)

The effects of length and shape of the aramid fibers on the mechanical properties of AFRC were investigated. Five types of aramid fibers of differing shapes and lengths were selected as specimens. Compression tests and direct tensile tests were conducted to determine the properties of plain concrete (PC) and AFRC.

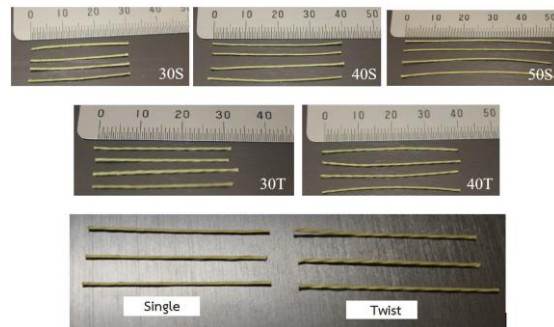
2.1 Material properties

Pictures of the fibers are presented in Figure 1a. The fibers included five types of aramid fibers with lengths of 30 mm, 40 mm, and 50 mm and different shapes of single (S) and twisted (T) fibers. The characteristics of each fiber type are summarized in Table 1. The specific lengths (L_f) tested in this

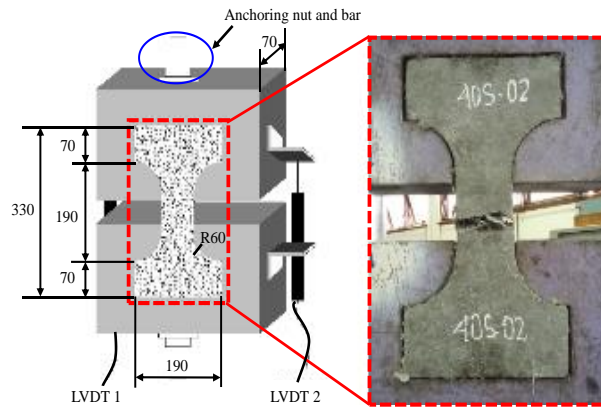
research study were 30 mm, 40 mm, and 50 mm. The aspect ratio (L_f/D_f) was equal to 60, 80, and 100. Table 2 presents the mix proportion designed for PC and AFRC. There were five mixes of AFRC with different fiber types (i.e., 30S, 40S, 50S, 30T, and 40T). The volume fraction of aramid fibers was 1.0% in the AFRC mixes.

2.2 Specimens and test setup

The 150x300 mm cylindrical specimens were prepared for the compression tests which were performed according to ASTM C-39 (2016). The dumbbell specimens with dimensions shown in Figure 1b were used for the direct tensile test. Direct tensile tests were undertaken to measure the tensile stress-displacement and ultimate tensile strength. Two displacement transducers were attached to each side of each specimen to monitor the elongation. The equipment setup used in the experimental program is shown in Figure 1b. For each experimental case, three replicates were tested and the average values were recorded.



(a) Geometry and shape of fibers



(b) Configuration of direct tensile test (Unit: mm)

Figure 1. Aramid fibers and direct tensile test setup.

Table 1. Properties and geometry of aramid fibers.

Specimens	Tensile strength (MPa)	Density (kg/m ³)	Length, L_f (mm)	Diameter, D_f (mm)	Aspect ratio, L_f/D_f	Shape
30S	3,307	1,390	30	0.5	60	Single
40S			40		80	Single
50S			50		100	Single
30T			30		60	Twisted
40T			40		80	Twisted

Table 2. Mix proportions of concrete and mortar.

Mix	w/b ¹⁾	Cement (kg/m ³)	Fly ash (kg/m ³)	Aggregate (kg/m ³)	Sand (kg/m ³)	Water (kg/m ³)	SP ²⁾ (g/m ³)	Aramid fiber (% Vol.)
PC	0.48	324.4	81.1	1016.5	827.7	194.8	1213.3	-
AFRC							3447.8	1.0
AFRM	0.40	628.7	-	-	1414.7	251.5	6287.4	1.0

¹⁾Water-binder ratio, ²⁾ Super plasticizer
 AFRC=Aramid fiber-reinforced concrete, AFRM=Aramid fiber-reinforced mortar

2.3 Effects of shape and length of the aramid fibers

2.3.1 Compressive strength

The results of the compressive strength tests of the investigated specimens are shown in Figure 2. The specimen with the single 30 mm fibers (30S) provided the highest compressive strength ($f_c'=41.2$ MPa). The compressive strengths of the concrete cylinders with 40S, 50S, 30T, and 40T were nearly similar. These observations may be due to the reasonable distribution of the aramid fibers in the specimen 30S that significantly triggered the stress transfer between the concrete and aramid. The experimental results also indicated that the compressive strength of AFRC was slightly lower than the specimen with PC except for the 30S-AFRC specimen. This implied that although the aramid fibers are a brittle material, the use of aramid fibers to reinforce concrete provided strength. Furthermore, the strength of the specimens with single aramid fibers decreased as the length of fibers increased (Figure 2). However, the specimens with twisted-shaped fibers resulted in a similar compressive strength as the fiber length increased. On the other hand, compared with the failure mode of the PC, the failure mode of the AFRC specimens resulted in a considerable change from fragile failure to ductile failure since a bridging effect of the fibers occurred in the AFRC specimens. Additionally, multiple fine cracks were visually observed in the AFRC specimens that meant that the stress transfer through the bridging effect was drastically activated.

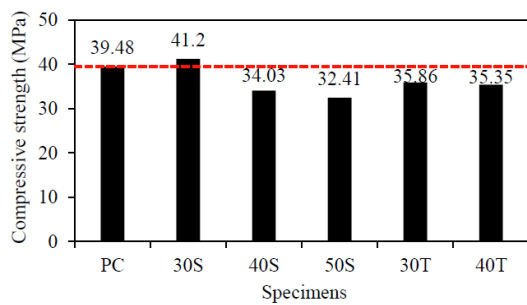
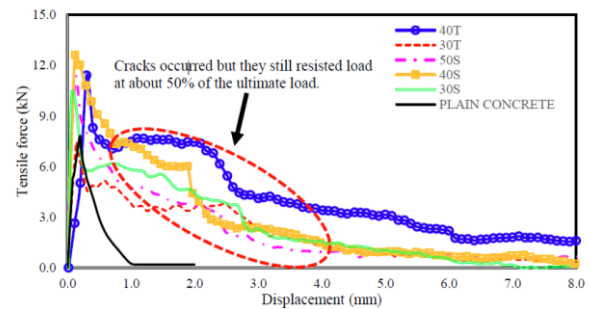


Figure 2. Compressive strength of PC and AFRC.

2.3.2 Direct tensile strength

Figure 3a presents the relationship of tensile force and displacement from the direct tensile test. It is obvious from Figure 3a that the PC specimen exhibited a brittle behavior during the test. However, the specimens reinforced by aramid fibers resulted in a ductile response since the absorption energy defined by the area under the curves of the



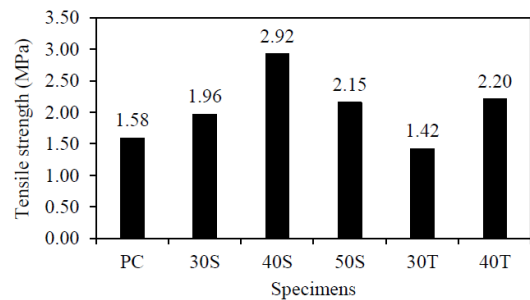
(a) Tensile force – displacement relationship



(b) Rupture failure of aramid fiber



(c) Pull-out failure of aramid fiber



(d) Direct tensile strength of tested specimens

Figure 3. Experimental results of direct tensile tests.

AFRC was higher than the PC specimen. Generally, the test revealed that an increase in the fiber length resulted in enhanced ductility because the fiber bridge connection induced stress activation in the AFRC specimens. Furthermore, the behavior of the specimens during the test was easily separated into two parts after the peak load. However, cracks occurred in the AFRC specimens, but they still resisted the loads due to the presence of the aramid fibers. The results indicated that the brittle tensile nature of the PC changed so that it became tough with the addition of the fibers. On the other hand, the maximum loads of the tested specimens occurred at deflections that ranged from 0.1 to 0.3 mm. After cracking, the load dropped and all AFRC specimens were able to resist the load at approximately 50–60% of the peak load and gradually decreased up to failure (Figure 3a). This means that the specimens with aramid fibers provided reasonable resistance to the applied load which made the specimens ductile. Then, the load decreased with increased displacement and the cracks could be constrained by the fibers up to very large displacement.

Additionally, there are two types of failure mode of the AFRC which were rupture of the aramid fibers and pull-out from the matrix as shown in Figures 3b and 3c, respectively. The rupture failure was displayed by branching fibers with many fiber filaments and the pull-out failure retained the original shape of the fibers. By observing the failure section of all 30 mm fiber experiments, it was observed that most of the fibers were pulled-out which indicated that the 30 mm fibers were not able to provide sufficient embedded length in the concrete. By inspecting the failed section of 40 mm fibers, it was observed that fiber failure was both rupture and pull-out which indicated that 40 mm fibers had sufficient embedded length in the concrete.

Figure 3d charts the direct tensile strength of the tested specimens which was calculated from the maximum tensile force. According to the experimental results, 40 mm fibers provided the highest tensile strength and the maximum tensile strengths were 2.2 and 2.92 MPa for the twisted and single fibers, respectively. Moreover, the tensile strength of the specimen with 50 mm fibers was lower than the specimen with 40 mm fibers (2.15 MPa vs. 2.92 MPa). In addition, in the post-peak region, the descending branch of the 50S specimen showed a downward trend until failure (Figure 3a). It should also be noted that balling was possibly a problem with increased fiber length which resulted in worse performance compared to the 40S specimen.

The results showed that in the case of fibers of the same length, the twisted fibers provided lower tensile strength than the single fibers because the twisted fibers were not perfectly straight (Figures 3a and 3d). Therefore, when stress occurred in the concrete, the twisted fibers were pulled to straighten and did not effectively resist the micro-cracks. On the other hand, the single fibers could immediately resist the propagation of cracks. However, the descending branch of the load-displacement curves of the twisted fibers was more stable than the single fibers. After displacement of approximately 1.5 mm was reached, the 40T specimen could resist more strength than the 40S because the twisted fiber provided a larger surface area for adhesion and frictional bond than the single fiber (Figure 3a). However, 30 mm twisted fibers did not clearly show this behavior because of insufficient length of the fibers. Therefore, based on its positive post-peak behavior,

40 mm twist fibers (40T) were selected and employed in the repair of corroded RC beams.

3. Investigation of Corroded RC Beams Repaired by AFRM and High Performance Mortar

3.1 Experimental program

3.1.1 Beam specimens

Four beams were tested under four-point bending. One beam without corrosion was the control beam (0C) and three beams were corroded using an accelerated corrosion process to reach 10% mass loss of longitudinal reinforcement (10C). Two corroded beams were repaired at the tensile zone using aramid fiber-reinforced mortar (AFRM) for one sample and high performance mortar (HPM) for the other (Table 3). The HPM, which is available in the market, is the mortar for spalled concrete resulting from reinforcement corrosion.

3.1.2 Specimen layout and detail

The details of the beams are presented in Figure 4a. Four beams with the same dimension (150×200×1400 mm) were prepared with cover concrete of 20 mm on all sides. Two longitudinal reinforcements consisted of 16-mm deformed bars (DB16) were arranged at the tension zone, and two 6-mm round bars (RB6) were arranged at the compression section for each beam. The stirrups were 9-mm round bars (RB9) with a spacing of 60 mm.

3.1.3 Materials

The compressive strength of the concrete was 32 MPa. The yield strength and ultimate strength of the 16 mm deformed steel bars were 537.15 MPa and 673.93 MPa, respectively. AFRM was used as the repair material with the mix proportion presented in Table 2. The 40T aramid fibers were used because they provided the best post-peak behavior. The compressive strength of the AFRM after 14 days was 56.5 MPa. The average tensile strength of the three dumbbell briquettes was 2.82 MPa (Table 3). The water to powder ratio for the HPM was 1:7 by weight according to the product data sheet. The compressive strength and tensile strength of the HPM were 32.7 MPa and 1.40 MPa, respectively (Table 3).

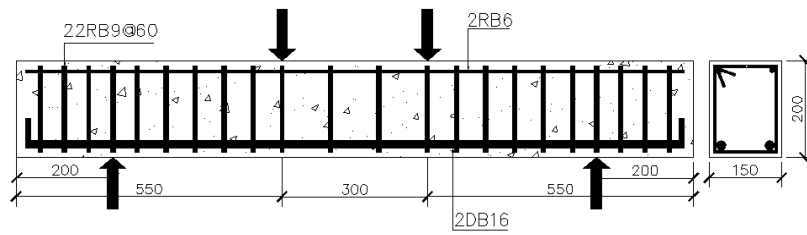
3.1.4 Accelerated corrosion and repairing procedures

Figure 4b shows the facility required for the process of accelerated corrosion. The main reinforcement was connected to the power supplies with lead wires. Specimens were submerged one-third of the way into 3% NaCl solution. Table 3 summarizes the total time and electric current for each beam. The cracking damage in the beams was observed after the accelerated corrosion process. The damaged concrete, which was 60 mm from the extreme tension fiber, was destroyed (Figure 4c). The rust around the reinforcing bars was removed by submerging the corroded steel bar in 10% diammonium hydrogen citrate at 60 °C for 2 days (JCI, 2004). After that, the repair processes were conducted on two beams (10C-AFRM and 10C-HPM) by cleaning the surface and

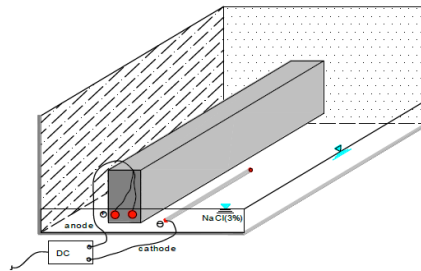
Table 3. Experimental program of beam repair.

Beam ID	Hour x Ampere (Ah)	Corrosion ratio (Mass loss)		Repaired by	Concrete		Repair material	
		Target	Actual		f_c' (MPa)	f_c' (MPa)	f_t (MPa)	
0C	-	-	-	-	-	-	-	-
10C	592	10%	10.0%	-	32.0	-	-	-
10C-AFRM	600	10%	9.2%	AFRM	32.0	56.5	2.82	
10C-HPM	602	10%	10.6%	HPM	32.0	32.7	1.40	

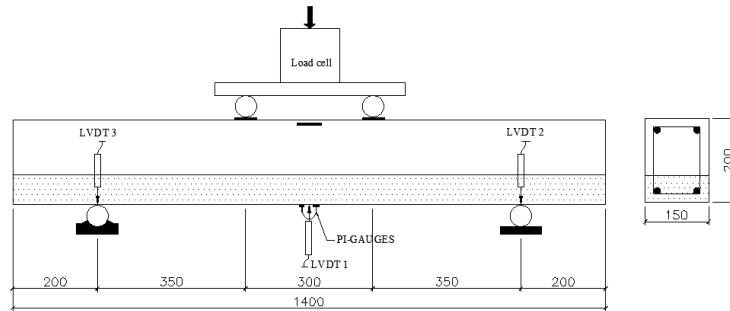
AFRM=Aramid fiber-reinforced mortar, HPM=High performance mortar.



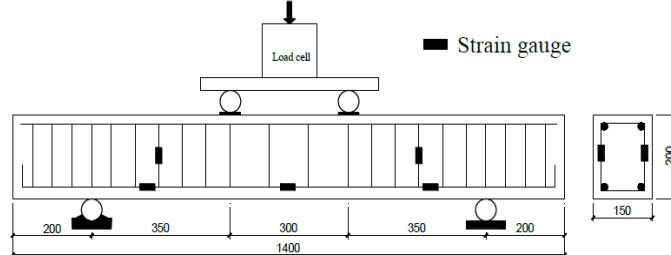
(a) Beam configurations



(b) Accelerated corrosion setup



(c) Test setup



(d) Locations of strain gauges

Figure 4. Details of beam specimens (unit: mm).

applying a bonding agent (LANKO 751) at the interface between the old concrete and repair materials. The patch repair was then done with 14 days of curing.

At the final phase after the bending tests, the reinforcements were taken off to measure the mass loss of the corroded bars (Figure 5a). The mass of the corroded longitudinal bars was compared to un-corroded longitudinal bars. The actual corrosion ratios are presented in Table 3. The measurements indicated that the corroded reinforcements had a mass loss of approximately 10%.

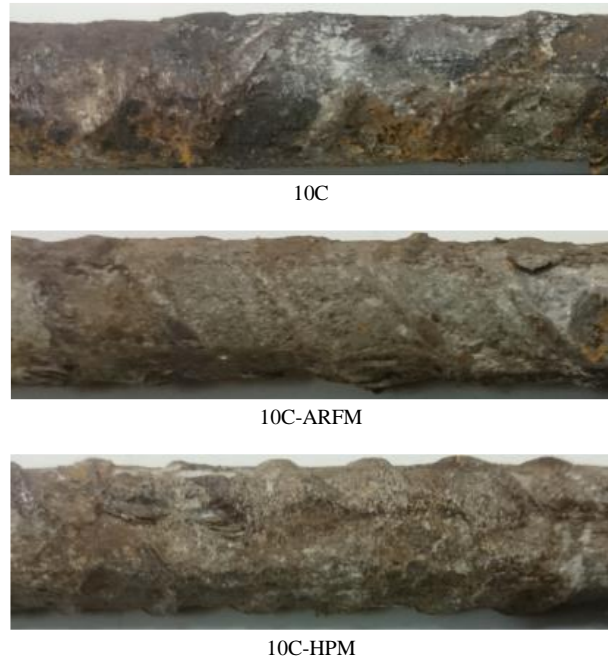
3.1.5 Test method

Figure 4c illustrates the experimental setup. Linear variable differential transducers were set at the mid-span and at the supports to measure the vertical displacements. A crack displacement transducer (PI-gauge) was attached at the bottom of each beam. Concrete strain gauges were attached at the compressive zone to measure compressive strain at the middle of the beam. Strain gauges were also attached on the longitudinal bars and stirrups (Figure 4d).

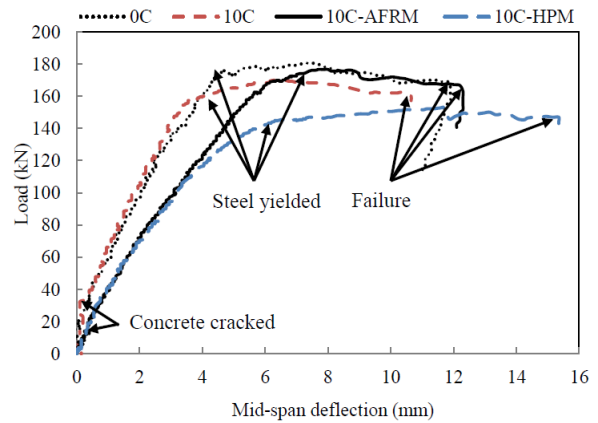
3.2 Experimental results and discussion

3.2.1 Load-deflection relations and failure mechanism

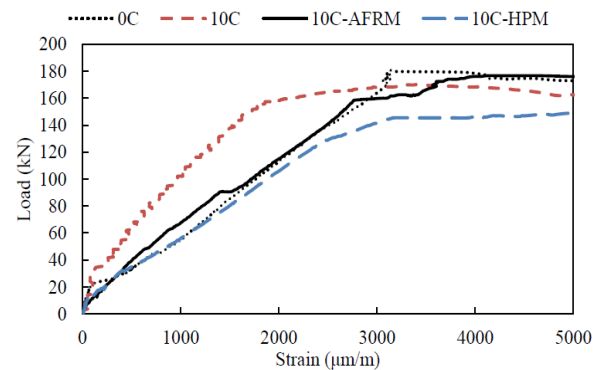
The load-deflection behavior of the beams consisted of three stages of pre-cracking stage, pre-yielding, and post-yielding until failure (Figure 5b). These stages are separated by the cracking and yielding load. Table 4 summarizes the results of cracking, yielding, ultimate load, and deflection of each beam. The cracking load is defined as the load at which flexural cracking is initiated. The cracking load was identified through observation during the test. The yield load is defined as the load at which the tensile steel yielded. Indeed, at the pre-cracking stage, the stiffness results of both the 0C and 10C beams were the same, while the stiffness results of the repaired beams (10C-AFRM and 10C-HPM) was relatively lower than the control beam (Figure 5b). The cracking load of 10C-AFRM was comparable with the 0C and 10C (Table 4). The yield loads of the 10C, 10C-AFRM, and 10C-HPM beams decreased by 9%, 6%, and 22%, respectively, compared to the control beam (0C). The yield load of the beam repaired using the AFRM was about 3% greater compared to the 10C beam without repair. This occurred because the aramid fibers helped to resist some tension force; thus, the yielding was delayed. On the other hand, the yield load of the 10C-HPM decreased about 15% compared to that of 10C because the high stiffness of the repaired HPM caused redistribution of the stress which resulted in the lower yielding load of the 10C-HPM specimen. After yielding, the load slightly increased before reaching the ultimate load. The control beam provided the highest load capacity among the four beams. Compared to the control beam, the ultimate loads decreased 6%, 2%, and 16% for the 10C, 10C-AFRM, and 10C-HPM beams, respectively. The load capacity of the 10C-AFRM was nearly the same as the load capacity of the control beam. However, repair using the HPM (10C-HPM) did not increase the load capacity of the beam. In addition, based on the absorption energy values displayed in Table 4, the 10C-HPM exhibited the greatest ductility compared to the other



(a) Surface of corroded bars



(b) Load-deflection relationships



(c) Load-reinforcement strain relationships

Figure 5. Experimental results of beam tests.

Table 4. Summary of test results.

Beam ID	Crack state		Yielding state		Ultimate state		Absorption energy (kN-mm)	Failure mode
	Load (kN)	Δ_{cr} (mm)	Load (kN)	Δ_y (mm)	Load (kN)	Δ_u (mm)		
0C	35	0.4	172.0	4.45	180.8	7.40	903.08	Flexural failure (concrete crushing)
10C	40	0.5	157.3	3.55	170.4	6.55		
10C-AFRM	40	1.05	161.5	5.65	176.6	7.80		
10C-HPM	20	0.45	133.9	5.10	152.6	11.75		

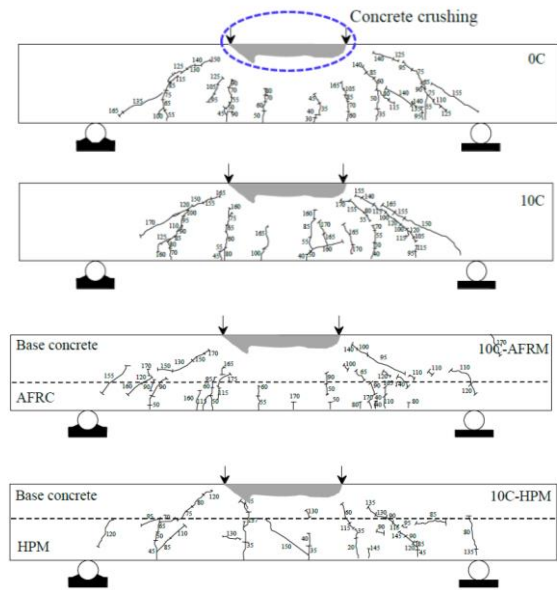
Note: Δ_{cr} is deflection at concrete cracking, Δ_y is deflection at yielding state, and Δ_u is deflection at ultimate state.

specimens. The specimens with the yielding load relative lower than the ultimate load resulted in better ductility defined by the absorption energy. This finding also agreed well with a study by Linh *et al.* (2018). The effectiveness of the beam repaired by AFRM was greater not only in the load capacity improvement but also in the ductility compared to the 10C beam.

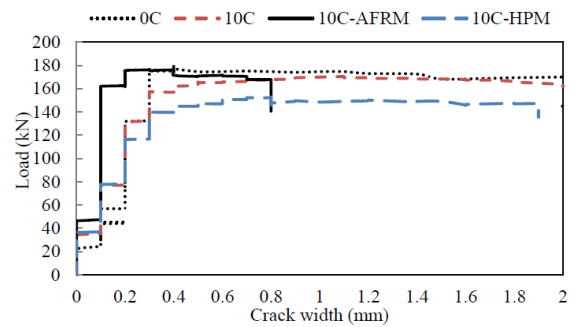
It was found that all steel bars yielded before the ultimate load (Figure 5c). The strain in the longitudinal bar of the 10C beam was rather low compared to the other beams (Figure 5c). This was possibly the result of bond deterioration between the concrete and the corroded bars. On the other hand, the bonding conditions of the bars in the 10C-AFRM and 10C-HPM were better than the 10C beam since the rust and the damaged concrete of these two beams were removed and patched with repair materials. Therefore, the strain of the bars in these specimens was similar to that of the control beam (0C). After exceeding the ultimate load, the load dropped due to crushing of the concrete in the compression zone. As a result, all four beams exhibited a reasonable failure mode of the concrete crushing in the compression zone.

3.2.2 Cracks pattern and crack width

The crack pattern of 0C was symmetrical with respect to the y-axis at the mid-span (Figure 6a). The flexural cracks initiated first at the mid-span, followed by cracks in the shear span, and then uniform crack spacing appeared. With an increase in load, the flexural cracks propagated vertically into the compression zone and, ultimately, crushing of the concrete occurred at failure of the beam. Flexural cracks were also observed on the non-repaired corroded beam (10C). However, due to the corrosion effect, which resulted in variation in the area of longitudinal bars, the crack pattern was not symmetrical. In the specimen repaired with AFRM, many fine cracks were observed. The crack width of 10C-AFRM was significantly smaller than the other beams because of the presence of fibers in the tension zone of the beam which limited the triggering of cracking through the fiber bridge. Some small horizontal cracks were also observed near the repair interface. These findings implied that the toughness of the beam repaired with AFRM was enhanced. On the other hand, the crack pattern of the 10C-HPM beam was different compared to the other beams. Few flexural cracks were observed. Also, the crack spacing increased and horizontal cracks near the interface were observed which were most likely due to the stiffness of the HPM which affected the stress distribution in the beam.



(a) Cracks patterns at ultimate load (the numbers next to cracks indicate the corresponding applied load in kN)



(b) Load-crack width relationship

Figure 6. Crack properties.

Figure 6b shows the width of the cracks from the PI-gauge at the middle bottom face of each beam. As expected, the same load-crack width relationship was found for each of the four beams at the first stage (0 to 22 kN). The 10C and 10C-HPM beams had the same load-crack width relationship at the second stage (38 kN to 117 kN). For the 10C-AFRM

beam, the crack width was significantly reduced from the load of 80 kN up to its ultimate state (176.6 kN) due to the presence of AFRM in the tension zone of the beam. This meant that the corroded RC beam repaired by AFRM provided an improvement of the safety requirement due to the small crack widths that occurred during the test which enhanced the serviceability of the beam in aggressive environments.

4. Conclusions

An improvement in the tensile property was observed with the use of aramid fibers with a reasonable length in concrete. Fibers that were 30 mm in length were not able to provide sufficient embedded length in the concrete because the fibers mainly pulled-out at the peak load. Fibers that were 50 mm in length showed relatively lower tensile strength in the direct tensile test because of fiber balling. Fibers that were 40 mm in length provided the highest direct tensile strength. Furthermore, although the single fibers yielded the highest tensile strength, the twisted fibers were able to resist higher loads in the post-peak region. The flexural capacity of the repaired corroded beam using HPM, which is a mortar product in the market, decreased by 11% compared to the unrepaired corroded beam. A large crack width was observed before the ultimate stage which led to early yielding of the steel reinforcement. Repairing beams using only mortar cannot recover the flexural capacity of a corroded RC beam. The use of aramid fibers to repair corroded RC beams provides the capability to recover load capacity and ductility of RC beams. Repairing these beams with AFRM could slightly delay the yielding of longitudinal reinforcement, which induced good toughness of the beams. In addition, it was observed that the number of cracks increased but the width of the cracks significantly decreased in the corroded beam repaired with the AFRM. Therefore, the safety requirement of the structures was met.

Acknowledgements

This work was financially supported by the Thailand Research Fund (TRG5880231) and Grants for Development of New Faculty Staff, Ratchadaphiseksomphot Endowment Fund, Chulalongkorn University and AUN/SEED-Net. The authors gratefully acknowledge the material support from Teijin Polyester (THAILAND).

References

Altun, F., Haktanir, T., & Ari, K. (2007). Effects of steel fiber addition on mechanical properties of concrete and RC beams. *Construction and Building Materials*, 21(3), 654-661. doi:10.1016/j.conbuildmat.2005.12.006

- ASTM C39/C39M-16b (2016). Standard test method for compressive strength of cylindrical concrete specimens. ASTM International, West Conshohocken, PA, Retrieved from <https://www.astm.org>.
- Chung, L., Najm, H., & Balaguru, P. (2008). Flexural behavior of concrete slabs with corroded bars. *Cement and Concrete Composites*, 30(3), 184-193. doi:10.1016/j.cemconcomp.2007.08.005
- Iqbal, S., Ali, A., Holschemacher, K., Bier, T. A., & Shah, A. A. (2016). Strengthening of RC beams using steel fiber reinforced high strength lightweight self-compacting concrete (SHLSCC) and their strength predictions. *Materials Design*, 100, 37-46. doi:10.1016/j.matdes.2016.03.015
- Japan Concrete Institute (2004). Standard Collection of JCI. 91-105.
- Jongvivatsakul, P., Watanabe, K., Matsumoto, K., & Niwa, J. (2011). Evaluation of shear carried by steel fibers of reinforced concrete beams using tension softening curves. *Journal of Japan Society of Civil Engineers, Ser. E2 (Materials and Concrete Structures)*, 67(4), 493-507. doi:10.2208/jsejmc.67.493
- Kim, W., Kim, J., & Kwak, Y. K. (2016). Evaluation of flexural strength prediction of reinforced concrete beams with steel fibres. *Journal of Structural Integrity and Maintenance*, 1(4), 156-166. doi:10.1080/24705314.2016.1240522
- Linh, V. H. B., Boonchai, S., & Ueda, T. (2017). Mechanical performances of concrete beams with hybrid usage of steel and FRP tension reinforcement. *Computers and Concrete*, 20(4), 391-407. doi:10.12989/cac.2017.20.4.391
- Linh, V. H. B., Boonchai, S., & Ueda, T. (2018). Ductility of concrete beams reinforced with both fiber-reinforced polymer and steel tension bars. *Journal of Advanced Concrete Technology*, 16(11), 531-548. doi:10.3151/jact.16.531
- Maaddawy, T. E., Soudki, K., & Topper, T. (2005). Long-term performance of corrosion-damaged reinforced concrete beams. *ACI Structural Journal*, 102(5), 649-656.
- Mansour, F. R., Pamiani, S., & Ibrahim, I. S. (2011). Experimental study on effects of steel fiber volume on mechanical properties of SFRC. *Advanced Materials Research*, 214, 144-148. doi:10.4028/www.scientific.net/AMR.214.144
- Soroushian, P., Bayasi, Z., & Khan, A. (1990). Development of aramid fiber reinforced cement composites. *ACI Special Publication*, 124, 79-98.
- Yoo, D. Y., Yoon, Y. S., & Banthia, N. (2015). Flexural response of steel-fiber-reinforced concrete beams: Effects of strength, fiber content, and strain-rate. *Cement and Concrete Composites*, 64, 84-92. doi:10.1016/j.cemconcomp.2015.10.001